Supporting Information

Layered indium chalcogenidoantimonates $[Me_2NH_2]_2In_2Sb_2S_{7-x}Se_x$ (x = 0, 2.20, 4.20, 7) with tunable band gaps and photocatalytic properties

Kai-Yao Wang,[a,b] Mei-Ling Feng,[a] De-Nian Kong,[a] Shi-Jing Liang,[c] Ling Wu,[c] and Xiao-Ying Huang*[a]

[a] *State Key Laboratory of Structural Chemistry, Fujian Institute of Research on the Structure of Matter, the Chinese Academy of Sciences, Fuzhou, Fujian 350002, P.R. China.*

[b] *Graduate School of the Chinese Academy of Sciences, Beijing 100049, P. R. China*

[c] *State Key Laboratory Breeding Base of Photocatalysis, Research Institute of Photocatalysis, Fuzhou University, Fuzhou, Fujian 350002, P.R. China.*

Fax: +86 591 83793727; Tel: +86 591 83793727; E-mail: xyhuang@fjirsm.ac.cn

1. Syntheses

Compound **1** was prepared from a mixture of In_2S_3 (0.163 g, 0.5 mmol), Sb_2S_3 (0.170 g, 0.5 mmol), S (0.048 g, 1.5 mmol) in a mixed solvent of *N,N*'-dimethylformamide (3mL) and hydrazine hydrate (99%, 0.8 mL) which was sealed in a stainless steel reactor with a 20 mL Teflon liner, heated at 160 ℃ for 5 days and then cooled to room temperature. The product contains lamellar orange crystals (**1**) and a little amount of indefinite orange powder. The crystals of **1** were selected by hand, washed by ethanol, and then dried in the air. The yield of the crystals of **1** is 0.284 g, 72% based on Sb. Anal. calc. for $[(Me)_2NH_2][In_2Sb_2S_7]$: C, 6.08%; H, 2.04%; N, 3.55%; S, 28.42%; Found: C, 6.25%; H, 1.90%; N, 3.50%; S, 28.85%.

Compound **2** was prepared from a mixture of In_2S_3 (0.163 g, 0.5 mmol), Sb_2S_3 (0.170 g, 0.5 mmol), Se (0.079 g, 1.0 mmol) in a mixed solvent of *N,N*'-dimethylformamide (3 mL) and hydrazine hydrate (99%, 0.6 mL) which was sealed in a stainless steel reactor with a 20 mL Teflon liner, heated at 160 ℃ for 5 days and then cooled to room temperature. The product contains lamellar pale brown crystals (**2**) and a little amount of indefinite black powder. The crystals of **2** were selected by hand, washed by ethanol, and then dried in the air. The yield of the crystals of **2** is 0.307 g, 69% based on Sb. Anal. calc. for $[(Me)_2NH_2][In_2Sb_2S_{4.80}Se_{2.20}]$: C, 5.38%; H, 1.81%; N, 3.14%; S, 17.24%; Found: C, 5.44%; H, 1.66%; N, 3.15%; S, 17.31%.

Compound **3** was prepared from a mixture of In_2S_3 (0.163 g, 0.5 mmol), Sb_2S_3 (0.170 g, 0.5 mmol), Se (0.158 g, 2.0 mmol) in a mixed solvent of *N,N*'-dimethylformamide (3 mL) and hydrazine hydrate (99%, 0.6 mL) which was sealed in a stainless steel reactor with a 20 mL Teflon liner, heated at 160 ℃ for 5 days and then cooled to room temperature. The product contains lamellar pale brown crystals (**3**) and a little amount of indefinite brown powder. The crystals of **3** were selected by hand, washed by ethanol, and then dried in the air. The yield of the crystals of **3** is 0.287 g, 58% based on Sb. Anal. calc. for $[(Me)_2NH_2][In_2Sb_2S_{2.80}Se_{4.20}]$: C, 4.87%; H, 1.63%; N, 2.84%; S, 9.10%; Found: C, 4.92%; H, 1.45%; N, 2.865%; S, 9.07%.

Compound **4** was prepared from a mixture of In (0.029 g, 0.25 mmol), Sb (0.029 g, 0.238 mmol), Se (0.081 g, 1.0 mmol) in a mixed solvent of *N,N*'-dimethylformamide (3 mL) and hydrazine hydrate (99%,

0.5 mL) which was sealed in a stainless steel reactor with a 20 mL Teflon liner, heated at 160 ℃ for 5 days and then cooled to room temperature. The product contains lamellar dark red crystals (**4**) and a little amount of indefinite brown powder. The crystals of **4** were selected by hand, washed by ethanol, and then dried in the air. The yield of the crystals of **4** is 0.112 g, 77% based on Sb. Anal. calc. for $[(Me)_2NH_2][In_2Sb_2Se_7]$: C, 4.30%; H, 1.44%; N, 2.51%. Found: C, 4.48%; H, 1.20%; N, 2.54%.

2. Crystal Structures

Single –crystal X-ray diffraction data were collected on a Rigaku Mercury CCD diffractometer for **1** and a Xcalibur E Oxford diffractometer for **2**, **3** and **4** with graphite monochrochromated Mo$K\alpha$ radiation (λ = 0.71073 Å) at room temperature. The absorption corrections were applied using multi-scan technique. The structures of these four compounds were solved by direct methods and refined by full-matrix least-squares on F^2 using the SHELXL-97 program.[1] Non-hydrogen atoms were refined anistropically, and the hydrogen atoms bonded to C and N atoms were positioned with idealized geometry. As for **2** and **3**, initial refinements confirmed that all the four crystallographically independent chalcogenide sites contain both Se and S with different ratios and the overall refined S:Se ratios are close to the EA results. Finally, the overall S:Se ratio in **2** and **3**, are restrained by SUMP restraint to be 4.80/2.20 and 2.80/4.20, respectively, according to the EA results. The formulae of **2** and **3** were also confirmed by thermogravimetric analysis (TGA) and energy-dispersive X-ray analysis (EDX) results. The relevant crystallographic data and structure refinement details, and the selected bond lengths and angles of four compounds can be found in Tables S1 and S2, respectively. Selected hydrogen-bonding data of **1**-**4** are given in Table S3.

Reference

1 G. M. Sheldrick, *SHELXS97 and SHELXL97*, University of Göttingen, Germany, 1997.

Table S1. Summary of data collections and structure refinements for crystals **1**, **2**, **3** and **4**.

	1	**2**	**3**	**4**
Empirical formula	$C_4H_{16}In_2N_2S_7Sb_2$	$C_4H_{16}In_2N_2S_{4.8}Sb_2Se_{2.2}$	$C_4H_{16}In_2N_2S_{2.8}Sb_2Se_{4.2}$	$C_4H_{16}In_2N_2Sb_2Se_7$
Formula weight	789.75	892.93	986.73	1118.05
Crystal system	monoclinic	monoclinic	monoclinic	monoclinic
Space group	*C2/c*	*C2/c*	*C2/c*	*C2/c*
T/K	296	296	296	296
λ/ Å	0.71073	0.71073	0.71073	0.71073
a/ Å	19.8124(6)	20.0561(16)	20.2182(19)	20.3648(11)
b/ Å	6.96070(10)	7.0325(3)	7.1175(3)	7.1872(2)
c/ Å	16.8179(4)	16.8343(16)	16.974(3)	17.1677(15)
β/º	123.610(17)	123.485(12)	123.619(14)	123.551(9)
V/ Å^3	1931.6(4)	1980.3(4)	2034.1(5)	2094.1(2)
Z	4	4	4	4
D_c/ Mg·m^{-3}	2.716	2.995	3.222	3.546
μ/mm^{-1}	5.864	9.532	12.654	16.879
F(000)	1464	1622	1766	1968
Measured refls.	7084	6427	4660	3977
Independent refls.	2217	2097	2146	2162
No. of parameters	80	84	84	80
GOF	1.071	1.057	1.052	1.011
R_1, wR_2 [$I > 2\sigma(I)$]:	0.0338, 0.0833	0.0471, 0.1212	0.0390, 0.0596	0.0253, 0.0407
R_1, wR_2 (all data)	0.0384, 0.0875	0.0586, 0.1329	0.0611, 0.0659	0.0393, 0.0415

[a] $R_1 = \sum||Fo|-|Fc||/\sum|Fo|$, $wR_2 = \{\sum w[(Fo)^2 - (Fc)^2]^2/\sum w[(Fo)^2]^2\}^{1/2}$

Table S2. Selected bond lengths (Å) and angles (°) for compounds **1**-**4** [a]

	1	**2**	**3**	**4**
Sb(1)-Q(2)	2.4386(12)□	2.4949(15)□	2.5361(12)□	2.5746(7)□
Sb(1)-Q(3)	2.4458(12)□	2.5062(15)□	2.5515(10)□	2.5809(7)□
Sb(1)-Q(4)	2.4474(13)□	2.5083(15)□	2.5536(11)□	2.5809(7)□
In(1)-Q(1)	2.4446(11)□	2.4781(15)□	2.5144(11)□	2.5663(6)
In(1)-Q(3)#1	2.4599(13)□	2.5040(15)□	2.5476(11)□	2.5751(7)
In(1)-Q(4)#2	2.4665(14)□	2.5198(16)	2.5600(12)	2.5797(8)
In(1)-Q(2)	2.4717(12)□	2.5086(15)□	2.5518(12)	2.5840(8)
Q(1)-In(1)#3	2.4446(11)□	2.4781(15)□	2.5144(11)□	2.5663(6)
Q(3)-In(1)#1	2.4599(13)□	2.5040(15)□	2.5476(11)□	2.5751(7)
Q(4)-In(1)#2	2.4665(14)□	2.5198(16)□	2.5600(12)□	2.5797(8)
Q(2)-Sb(1)-Q(3)	97.67(5)□	97.79(5)□	97.81(4)□	97.68(2)
Q(2)-Sb(1)-Q(4)	94.19(5)□	93.36(5)□	93.09(4)□	92.97(2)
Q(3)-Sb(1)-Q(4)	94.46(4)□	94.55(5)□	94.53(4)□	95.19(2)
Q(1)-In(1)-Q(3)#1	120.07(4)□	119.85(6)□	120.01(4)	120.66(2)
Q(1)-In(1)-Q(4)#2	99.83(5)□	99.67(6)□	99.52(4)	99.75(2)

Q(3)#1-In(1)-Q(4)#2	108.17(5)□	107.66(5)□	107.71(4)	107.86(3)
Q(1)-In(1)-Q(2)	109.31(4)□	108.73(4)	108.94(4)	109.03(2)
Q(3)#1-In(1)-Q(2)	106.47(4)□	107.13(5)	106.76(4)	106.07(2)
Q(4)#2-In(1)-Q(2)	113.12(4)□	113.95(5)	114.10(4)	113.68(2)
In(1)-Q(1)-In(1)#3	113.23(7)□	110.62(10)	109.10(6)	107.89(3)
Sb(1)-Q(2)-In(1)	97.85(5)□	96.12(5)	95.13(4)	94.55(2)
Sb(1)-Q(3)-In(1)#1	96.00(4)□	94.36(5)	93.42(4)	93.34(2)
Sb(1)-Q(4)-In(1)#2	96.22(5)□	94.73(5)	94.49(4)	94.65(3)

[a]Q = S for **1**; Q = S/Se for **2** and **3**; Q = Se for **4**; Symmetric codes for **1-4**: #1 -*x*,-*y*,-*z*+1;#2 -*x*,-*y*+1,-*z*+1;#3 -*x*,*y*,-*z*+3/2.

Table S3. Selected hydrogen bonds data for **1-4** [a].

D-H...A	d(D-H)(Å)	D(H...A)(Å)	d(D...A)(Å)	<(DHA) (°)
$[(Me)_2NH_2][In_2Sb_2S_7]$ (**1**)				
N(1)-H(1A)···S(1)#2	0.90	2.54	3.365(6)	153.2□
N(1)-H(1B)···S(3)#4	0.90	2.84	3.569(6)	139.5□
C(2)-H(2B)···S(2)#5	0.96	2.85	3.811(7)	175.1□
$[(Me)_2NH_2][In_2Sb_2S_{4.80}Se_{2.20}]$ (**2**)				
N(1)-H(1A)···Q(1)#2	0.90	2.57	3.393(11)	152.5□
N(1)-H(1B)···Q(3)#4	0.90	2.86	3.619(12)	142.4□
C(2)-H(2B)···Q(2)#5	0.96	2.90	3.814(12)	160.4□
$[(Me)_2NH_2][In_2Sb_2S_{2.80}Se_{4.20}]$ (**3**)				
N(1)-H(1A)···Q(1)#2	0.90	2.54	3.385(9)	156.3□
N(1)-H(1B)···Q(3)#4	0.90	2.94	3.679(10)	140.3□
C(2)-H(2B)···Q(2)#5	0.96	2.90	3.832(11)	164.9
$[(Me)_2NH_2][In_2Sb_2Se_7]$ (**4**)				
N(1)-H(1B)···Se(1)#2	0.90	2.66	3.474(6)	151.0□
N(1)-H(1A)···Se(3)#4	0.90	2.89	3.656(7)	144.4□
C(2)-H(2B)···Se(2)#5	0.96	2.93	3.882(8)	173.3□

[a]Q = S/Se for **2** and **3**; Symmetry codes: #1 -*x*, -*y*, -*z*+1; #2 -*x*, -*y*+1, -*z*+1; #3 -*x*, *y*, -*z*+3/2; #4 -*x*+1/2, -*y*+1/2, -*z*+1; #5 *x*, -*y*+1, *z*-1/2.

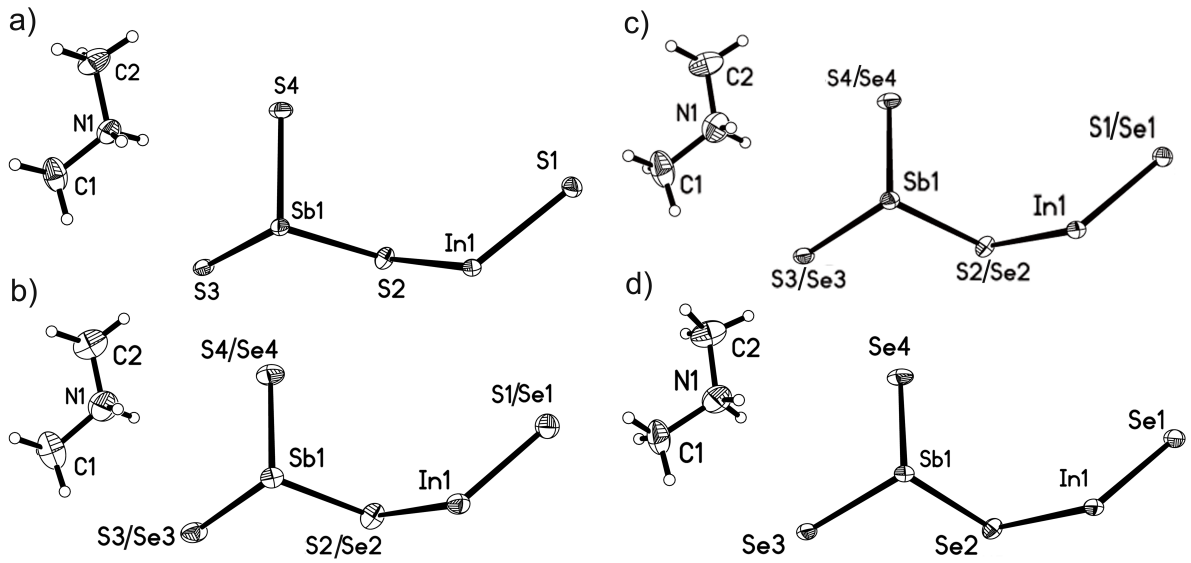

Fig. S1 *ORTEP* plots showing the crystallographically asymmetric units in **1** (a), **2** (b), **3** (c) and **4** (d) with labeling scheme and 30% probability level.

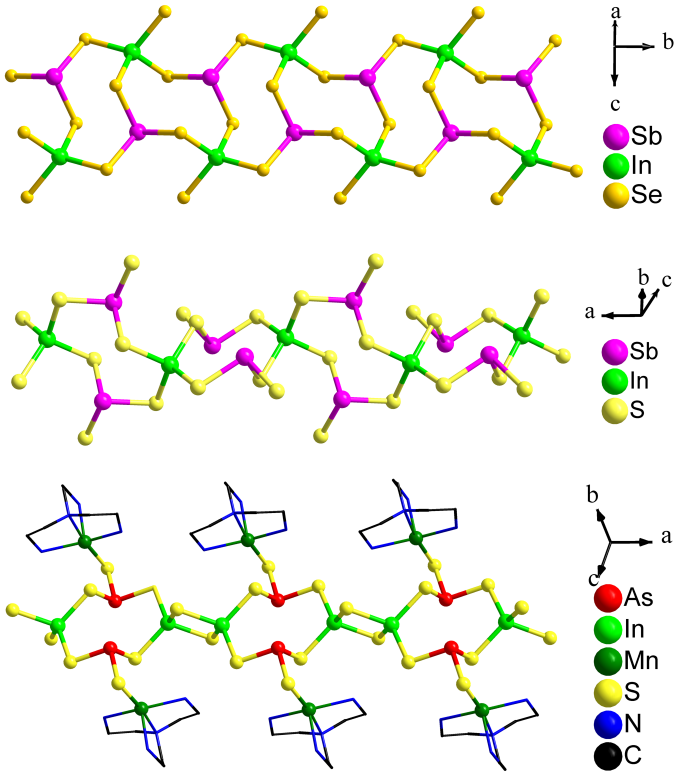

Fig. S2 Comparison of the connection modes of $\{In_2Sb_2Se_{10}\}$ clusters in **4** (a) and that of the similar $\{In_2M_2S_{10}\}$ (M = Sb, As) clusters in the reported $[In_2Sb_2S_8^{4-}]_n$ (b) and Mn(tren)InAsS$_4$ (tren = tris(2-aminoethyl)amine) (c).

3. Characterization

All analytical grade chemicals employed in this study were commercially available and used without further purification. Elemental analyses (C, H, N and S) were performed using a German Elementary Vario EL III instrument. SEM images and energy-dispersive X-ray analysis (EDXA) were obtained with a JEOL JSM-6700F scanning electron microscope. FT-IR spectra (KBr pellets) were recorded on an ABB Bomen MB 102 spectrometer. The UV/Vis spectra were measured at room temperature using a PE Lambda 900 UV/Vis spectrophotometer, and a $BaSO_4$ plate was used as a standard (100% reflectance). The absorption spectra was calculated from reflectance spectra by using the function give by Tauc: $(\alpha E)^{1/2}= A(E-E_g)$ where α is the absorption coefficient, E is the photon energy and E_g is the optical band gap. Powder X-ray diffraction (PXRD) patterns was recorded in the angular range of 2θ = 3-65° on a Miniflex II diffractometer using Cu$K\alpha$ radiation. Thermogravimetric analyses were carried out with a NERZSCH STA 449C unit at a heating rate of 5 ℃/min under a nitrogen atmosphere.

Reference

1 J. Tauc, *The optical properties of solids*, Amsterdam, 1970.

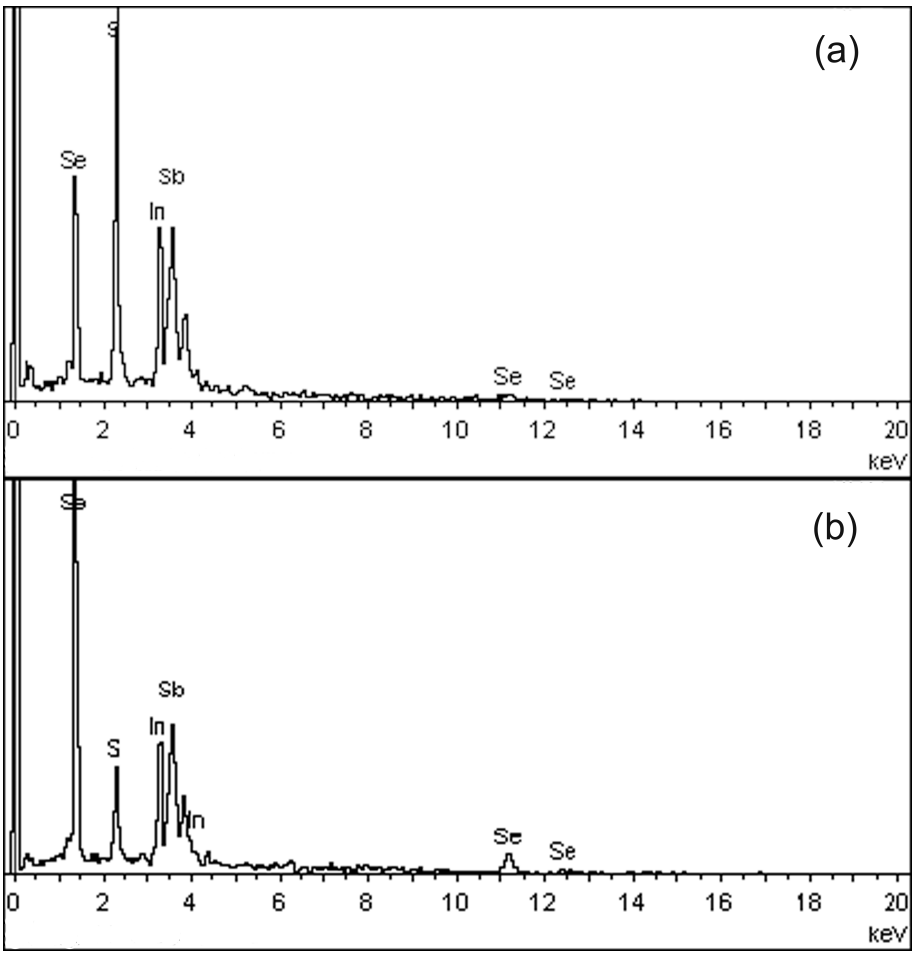

Fig. S3 The energy dispersive spectroscopy (EDS) of **2** (a) and **3** (b). Data collected on four samples of **2** and four samples of **3** confirmed that the average In: Sb: S: Se ratios were 2/2.04/4.92/2.66 for **2**, and 2/1.99/2.17/5.07 for **3**, respectively.

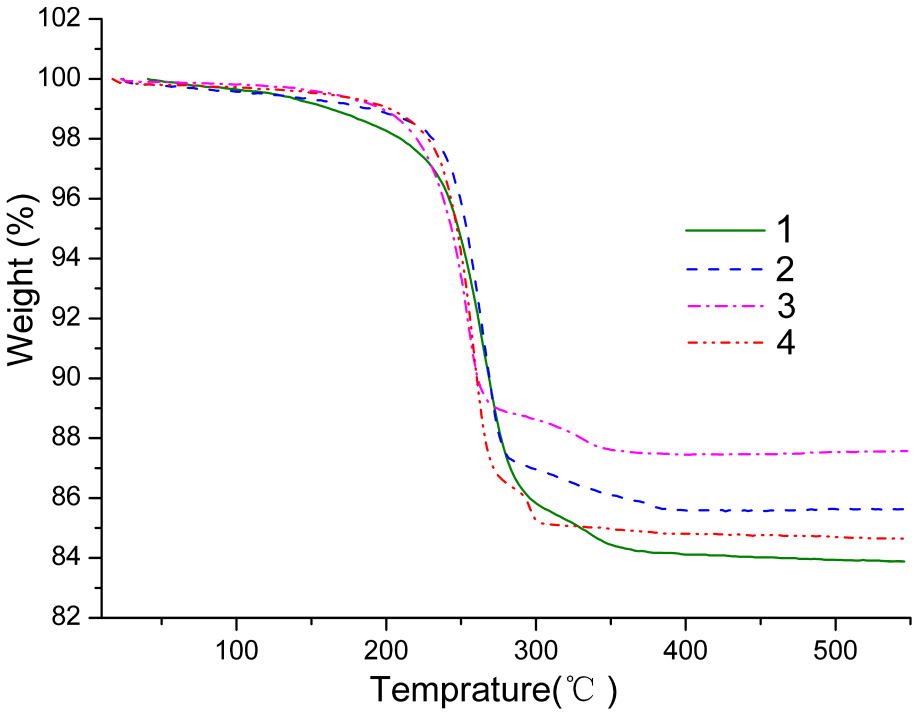

Fig. S4 Thermogravimetric curves for **1**, **2**, **3** and **4**.

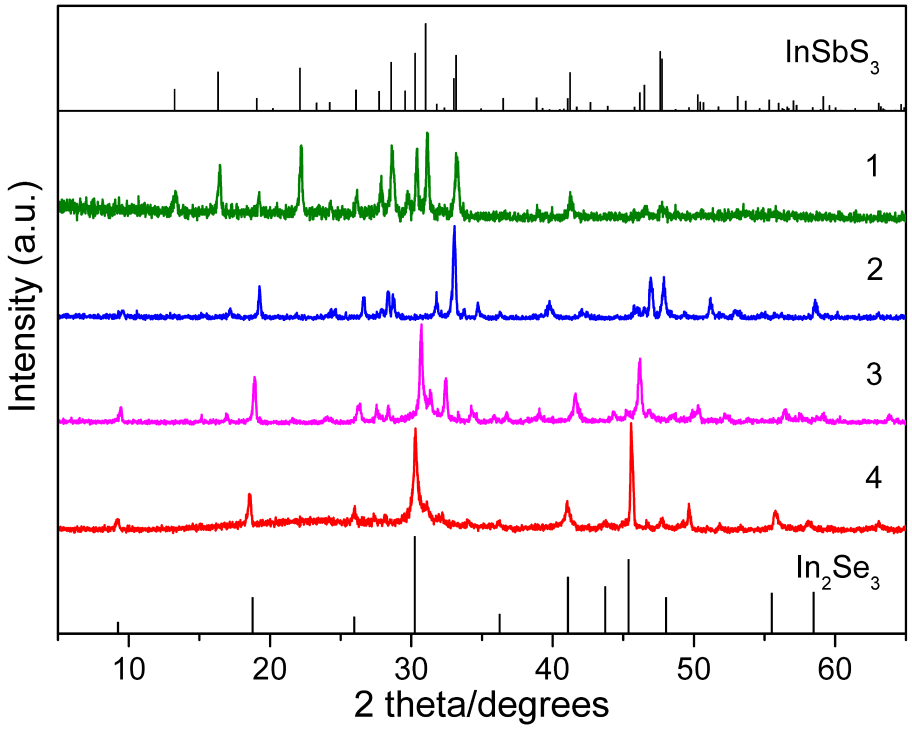

Fig. S5 The PXRD patterns of the TG residues of **1**, **2**, **3** and **4**. It indicates that the final residue of **1** is $InSbS_3$, while the residue of **4** is In_2Se_3 with an indefinite crystalline phase. The residues of **2** and **3** both are $In_2S_xSe_{3-x}$ solid solutions and indefinite crystalline phases.

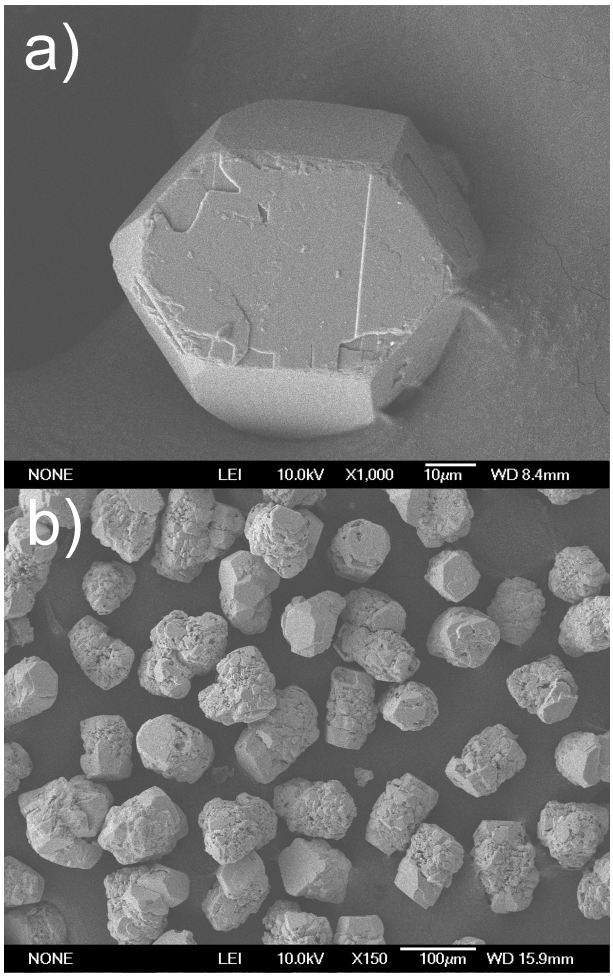

Fig. S6 SEM images of (a) a single crystal, and (b) the polycrystals of sample **4**. We could see clearly that the shape of the crystal is hexagonal plate and the polycrystalline sample is monodisperse particles, whose grain size is about 100 μm.

4. Photocatalytic activity measurements

The photocatalytic reactions under UV irradiation for the degradation of the MO were performed in a quartz tube with 4.5 cm inner diameter and 17.5 cm length. Three 4 W UV lamps (Philips, TUV 4W/G4 T5) with a wavelength centered at 254 nm were used as illuminating source. 120 mg of powdered photocatalysts were suspended in 200 mL MO (10 mg/L) aqueous solution and stirred for 55 min in dark before irradiation to reach the adsorption/desorption equilibrium. About 5 mL suspension was continually taken from the reaction cell at 20 min intervals during the irradiation and centrifuged (Anke, TGL-16C). The resulting solution was analyzed on a PE Lambda 900 UV/Vis spectrophotometer. The percentage of degradation is reported as C/C_0, where C is the main peak of the absorption of methyl orange at each irradiated time interval at wavelength 464 nm and C_0 is the absorption of the starting concentration when adsorption/desorption equilibrium was achieved (see Fig. 4a in the paper).

The photocatalytic reactions under visible irradiation (400~800 nm) for the degradation of the MO were performed in a quartz tube with 4.5 cm inner diameter and 9.5 cm length. A 300 W tungsten halogen lamp (Philips) was positioned inside a cylindrical pyrex vessel and surrounded by a circulating water jacket to cool the lamp. Two cut-off filters were placed outside the Pyrex jacket to remove all wavelengths less than 400 nm and more than 800 nm, ensuring irradiation with visible-light only. 60 mg of powdered

photocatalysts were suspended in 100 mL MO (10 mg/L) aqueous solution and stirred for 55 min in dark before irradiation to reach the adsorption/desorption equilibrium. About 5 mL suspension was continually taken from the reaction cell at 1h intervals during the irradiation and centrifuged (Anke, TGL-16C). The resulting solution was analyzed on a PE Lambda 900 UV/Vis spectrophotometer. The percentage of degradation is reported as C/C_0, where C is the main peak of the absorption of methyl orange at each irradiated time interval at wavelength 464 nm and C_0 is the absorption of the starting concentration when adsorption/desorption equilibrium was achieved (See Fig. 4b in the paper).

The photocatalytic reactions under visible irradiation (600~780 nm) for the degradation of the MO were performed in a quartz tube with 4.5 cm inner diameter and 9.5 cm length. The visible light for the photocatalytic reaction was generated with a 300 W Xe lamp (PLS-SXE300C). Two cut-off filters were placed outside the Pyrex jacket to remove all wavelengths less than 600 nm and more than 780 nm, ensuring no irradiation can be absorbed by the MO. 30 mg of powdered sample **4** were suspended in 50 mL MO (10 mg/L) aqueous solution and stirred for 55 min in dark before irradiation to reach the adsorption/desorption equilibrium. About 4mL suspension was continually taken from the reaction cell at 2h intervals during the irradiation and centrifuged (Anke, TGL-16C). The resulting solution was analyzed on a PE Lambda 900 UV/Vis spectrophotometer. The percentage of degradation is reported as C/C_0, where C is the main peak of the absorption of methyl orange at each irradiated time interval at wavelength 464 nm and C_0 is the absorption of the starting concentration when adsorption/desorption equilibrium was achieved. The results are shown in the Fig. S8. Clearly, the MO could be degraded under this photocatalytic reaction process. The photodegradation rate was relatively low in the initial 8h "induction period". After that, there was an obvious acceleration of the photodegradation. Compared with the photodegradation results observed from Fig. 4(b) (light wavelength: 400~800 nm, shown in the manuscript), the degradation efficient is lower in the 600~780 nm case as shown in Fig. S8, which may be due to the weaker absorption of 600~780 nm for sample **4**, and the removal of photodegradation through the "indirect photocatalytic mechanism".

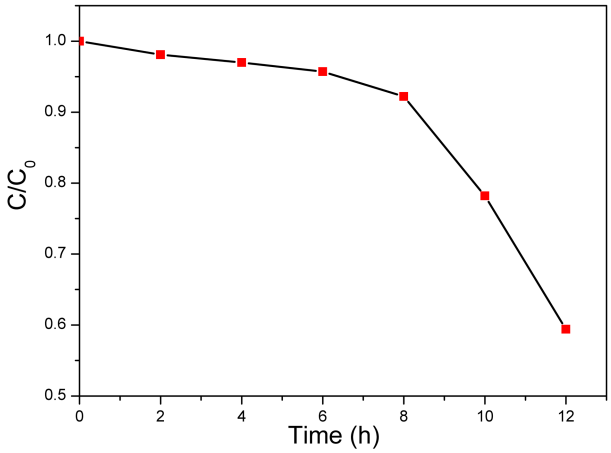

Fig. S7 Photodegradation of MO by sample **4** monitored as the normalized change in concentration as function of irradiation time under visible light (Xe lamp, 600~780 nm).

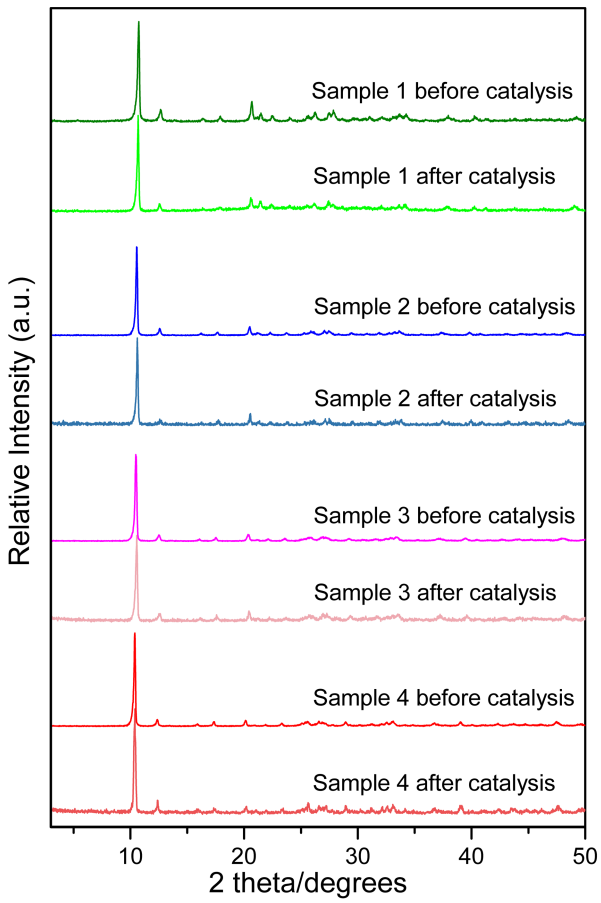

Fig. S8 XRD patterns of samples **1** and **2** before and after the 200 min UV photocatalysis and samples **3** and **4** before and after the 10h VIS photocatalysis. The XRD patterns of the catalysts before and after the photodegradation tests are essentially the same, implying stability of the four samples.